# The odontogenic performance of human dental pulp stem cell in 3-dimensional chitosan and nano-bioactive glass-based scaffold material with different pores size

Reham A.A. Morsy<sup>a</sup>, Hanan Beherei<sup>b</sup>, Marwa Ellithy<sup>a</sup>, Heba E. Tarek<sup>a</sup>, Mostafa Mabrouk<sup>b</sup>

<sup>a</sup>Oral Pathology, Basic Dental Science Department, Oral and Dental Research Division, <sup>b</sup>Refractories, Ceramics and Building Materials Department, National Research Center, Giza, Egypt

Correspondence to Reham A.A. Morsy, BSc, MSc, PhD in oral pathology, Faculty of Oral and Dental Medicine, Cairo University, Basic Dental Science Department, Oral and Dental Research Division, National Research Centre, 33 El Bohouth Street, 12622 Dokki, Cairo, Egypt. Tel: +201005016380;

fax: +20233387803; e-mail: rehammorsy77@yahoo.com

Received: 19 June 2019 Revised: 5 August 2019 Accepted: 6 August 2019

Published:

Journal of The Arab Society for Medical Research 2019, 14:82–94

#### **Background**

This study focused on the development of biocompatible and biodegradable homoporous chitosan scaffolds containing nano-bioactive glass 58S for dental tissue regeneration. For this aim, we developed a new chemical route to obtain homoporous scaffolds that mimic cancellous bone by utilizing  $H_2O_2$ .

#### Materials and methods

Different properties of the prepared powder of 58S were analyzed by transmission electron microscopy, thermogravimetric analysis (TGA)/differential scanning colometric (DSC), X-ray diffraction, and Fourier transform infrared spectroscopy. The developed scaffolds were analyzed by X-ray diffraction, Fourier transform infrared spectroscopy, and scanning electron microscope in comparison with heteroporous scaffolds prepared in the absence of  $H_2O_2$ . Stem cells from dental pulp were seeded onto the prepared scaffolds for different periods of time. The ability to differentiate toward an odontogenic lineage was studied for the loaded cells with the prepared scaffolds.

#### Results

The size of the prepared nano-bioglass 58S nanoparticles was in the range of 23.9–98.18 nm. The scaffolds prepared using  $H_2O_2$  exhibited homogenous porous scaffolds in the range of 250–450  $\mu m$  size when compared with scaffold synthesized in the absence of  $H_2O_2$ , which demonstrated heterogeneous scaffolds in the range of 350–700  $\mu m$ . The cell studies showed better cell growth and biomineralization with the heterogeneous scaffolds compared with homogenous microarchitecture.

#### Conclusion

The microarchitecture of heterogeneous scaffolds plays a significant role in dental pulp stem cell differentiation and calcified tissue development as well as provides new possibilities for dental tissue engineering.

#### **Keywords:**

biomineralization, cell growth, different porous chitosan scaffolds, pulp tissue, root canal treatment

J Arab Soc Med Res 14:82–94 © 2019 Journal of The Arab Society for Medical Research 1687-4293

#### Introduction

The most common irresistible infection among kids and grown-ups is dental caries. Approximately 90% of the total populace has encountered tooth decay [1]. Dental caries is described by tainted and necrotic dental pulp tissue. The tissue of dental pulp gives imperativeness and affects the ability of the tooth. Vascularization and tissue support are the main characteristics of the pulp tissue; in addition, it is also considered as stem cell source. Therefore, the pulp plays an important role in homeostasis and building of dentin recovery [2]. Root canal therapy remains the available clinical therapy for dental caries. The root canal treatment includes the decontamination and substitution of the diseased and destroyed tissue of pulp with a special mineral complex. Secondary infections and the complications may take place owing to the presence of this mineral complex [3].

In some cases, a significant complication could be observed such as inhibition of root maturation upon the treatment of root canal [4,5].

Recently, tissue engineering was explored significantly in the restoration of different hard tissues especially dental tissue [6–8]. It is currently realized that equalization should be accomplished between having scaffold pores sufficiently substantial to encourage cell infiltration while still little enough to permit a high clear surface area for cell attachment [4,5]. Numerous investigations have featured the effect of various sorts of scaffolds on the performance of pulp stem cells and the significance

This is an open access journal, and articles are distributed under the terms of the Creative Commons Attribution-NonCommercial-ShareAlike 4.0 License, which allows others to remix, tweak, and build upon the work non-commercially, as long as appropriate credit is given and the new creations are licensed under the identical terms.

of the surrounding environment to help cell-cell communications and tissue recovery. Nevertheless, to date, there are as yet contradicting hypotheses regarding the scope of which scaffolds' mean pore sizes are perfect for in-vitro odontogenesis [9–11].

The advancement of scaffolds having ideal qualities for the inducement of human dental pulp stem cells (HDPSCs) interceding odontogenesis utilizing the approach of tissue engineering is of incredible premium, so the aim of this study was to explore the adhesion, proliferation, and growth of HDPSCs on porous chitosan-based nano-composite scaffolds with Different pore sizes and to evaluate the differentiation of these cells toward an odontogenic lineage.

#### Materials and methods

#### **Materials**

Chitosan (molecular weight=2.46×105, degree of triethyl deacetylation=85%), phosphate  $C_6H_{15}O_4P$ ), ammonia solution (NH<sub>4</sub>OH), tetraethyl orthosilicate (TEOS: C<sub>8</sub>H<sub>20</sub>O<sub>4</sub>Si), calcium nitrate tetrahydrate [Ca (NO<sub>3</sub>)<sub>2</sub> · 4H<sub>2</sub>O], nitric acid (H<sub>2</sub>NO<sub>3</sub>) (NaOH), and sodium hydroxide were purchased from the Sigma-Aldrich (St. Louis, MO, USA). Hydrogen peroxide (H<sub>2</sub>O<sub>2</sub>) was purchased from Delta for Chemicals Co., Egypt.

#### Study design

The chitosan-based nano-composite scaffolds (with powder of 58S) were prepared and analyzed by transmission microscopy (TEM), electron thermogravimetric (TGA)/differential analysis scanning colometric (DSC), X-ray diffraction (XRD), and Fourier transform infrared spectroscopy (FTIR) spectroscopy in comparison with heteroporous scaffolds prepared in the absence of H<sub>2</sub>O<sub>2</sub>. HDPSCs were seeded onto the prepared scaffolds for different periods of time. The studied cases were divided into two groups according to pores size: homoporous scaffold, with range of 250-450 µm size, and heteroporous scaffold, with range of 350-700 µm. The ability of the stem cells to attach, proliferate, and differentiate toward an odontogenic lineage was studied for the loaded cells with the prepared scaffolds.

#### Ethical approval

All experiments were approved by the Ethical Committee of the National Research Center with approval number 16/340.

#### Preparation of 58S bioactive glass

The bioactive glass was synthesized with a system of 57.44% SiO<sub>2</sub>, 35.42% CaO, and 7.15% P<sub>2</sub>O<sub>5</sub> in molar (%), and it was selected according to the diagram of

ternary phase bioactive glass (CaO-SiO<sub>2</sub>-P<sub>2</sub>O<sub>5</sub>) [12]. Particularly, tetraethoxysilane (TEOS) (14.8 g) was hydrolyzed in 0.1 mol/l nitric acid (30 ml) for 30 min of continued agitation to ensure its complete hydrolysis. The resulted solution was topped up using distilled water till the solution turned into a transparent solution, and the final molar ratio for TEOS: H<sub>2</sub>O was 1 : 12. Triethyl phosphate (0.85 g) was added to the stirring solution after 30 min. Then 7.75 g of calcium nitrate was added after another 20 min, and the stirring was continued for another hour. This was followed by drying of the resulted mixture for overnight at 70°C and 2 days at 120°C in an oven. Heat treatment was conducted for the dried powder for 2h at 600°C to eliminate nitrates and to stabilize the glass.

## Fabrication of chitosan/nano-bioglass 58S porous

The porous scaffolds were prepared according to previous research with some modification [13]. The scaffolds were prepared by dispersion of 58S-BG nanopowders in 3% w/v chitosan solution dissolved using 1% v/v acidified distilled water or hydrogen peroxide (H<sub>2</sub>O<sub>2</sub>). Chitosan/BG nanocomposite matrix was put in a cylindrical mold and then kept in fridge at -20°C overnight till solidification. Afterward, lyophilization was initiated in the frozen scaffold using freeze-dryer at -80°C for 24 h. Finally, scaffolds were submerged in 3% w/v NaOH solution for normalization, and the NaOH residuals were removed carefully using deionized water.

#### Transmission electron microscopy

TEM was used to analyze the size and morphology of the fabricated nanopowders. The particle size and appearance of the prepared bioactive glass 58S were determined using TEM (JEM-2100; Jeol) at an accelerating voltage of 200 kV.

#### Thermodynamic behavior of nano-bioactive glass 58S

The thermal behavior of the prepared bioactive glass 58S was investigated by DSC/TGA using a computerized SETARAM Labsys TG-DSC thermal analysis system. Samples (100±1 mg) were placed in the 30-ml platinum crucible with a heating range of 25-1000°C with a heating rate of 10°C/min.

#### X-ray diffraction

XRD patterns of the powder were collected by using XRD (D8 ADVANCED Cu target; Bruker, USA) diffractometer. To produce monochromatic X-rays, a Cu Ka source was used with an emission current of 200 mA and a voltage of 40 kV with a wavelength of 0.1542 nm. The measurements were conducted in the range of  $2^{\circ}$ – $70^{\circ}$  at a scan speed of  $4^{\circ}$ /min.

#### Fourier transform infrared spectroscopy

To investigate the functional groups of the prepared nano-bioactive glass 58S and nanocomposite scaffolds, FTIR was implemented. KBr disks of 0.5-cm diameter were prepared after mixing with the tested samples (mixing ratio 1 : 100 sample: KBr) in the mortar and grinded into a fine powder. Perkin Elmer Spectrum 2000 FTIR spectrometer Demonstrate 1600, Perkin-Elmer (USA), was utilized to record FTIR spectra at a resolution of 4 cm<sup>-1</sup>.

## Scanning electron microscope and elemental X-rays analysis

Scanning electron microscope (SEM) was utilized to study the sample surfaces, alongside energy-dispersive X-ray spectrometry (EDS) for evaluating the sample surface. SEM examination was attempted utilizing a Jeol JXA-840A, Electron Probe miniaturized scale analyzer (Japan), at 15 kV. Samples were rendered electrically conductive before examination through gold-sputter covering (SPI Module Sputter Coater; SPI Supplies, West Chester, Pennsylvania, USA) and were appended to the SEM stub utilizing glue carbon tape.

#### Porosity (%) by liquid displacement method

The porosity (%) of the fabricated scaffolds was evaluated after their submersion in cyclohexane for 1 h, as reported earlier [14]. Based on the liquid displacement method, in which the scaffold volume equals the volume of the displaced fluid, the porosity (%) could be calculated from Eq. (1).(1)

$$P\left(\%\right) = \left[ \frac{W1 - W3}{W2 - W3} \right] \times 100,$$

the symbol W1 is attributed to the scaffold dry weight, W2 the scaffold weight after 1 h of immersion, and W3 is the scaffold dried weight after removing the scaffold from the cyclohexane. From this equation, porosity percentage (P %) could be determined.

#### Scaffolds degradation in simulated body fluid

To determine the degradation (%) of the scaffolds, they were soaked in simulated body fluid (SBF) (pH 7.4) at 37°C in the thermostatic incubator up to 28 days [15]. All composite scaffolds (three equal pieces) from each sample were immersed in SBF. Before submerging the scaffold in SBF, its weight was determined as Wi. After 28 days of soaking in SBF, the scaffolds were removed from SBF, washed three times with distilled water to stop the ions adsorption on the surface of the scaffolds

and air dried. Then, all scaffolds were weighted and recorded (Wt); the mass loss was estimated by Eq. (2). Mass loss (%) was registered as mean±SD (n=3).(2)

$$Mass \, loss \, (\%) = \left\lceil \! \frac{Wi - Wt}{Wi} \! \right\rceil \times 100. \label{eq:mass_mass_mass}$$

#### In-vitro analysis

Primary HHDPSCs were isolated from sound third molar indicated for extraction in a healthy adult patient after NRC ethics committee approval (16/340). According widely established to protocols, HHDPSC isolation was carried out [16]. Cells were suspended at a density of 5×10<sup>6</sup> cells/ml, with a total volume of 100 µl per scaffold. In brief, 9.5-mm diameter, 4-mm height scaffolds were prehydrated in PBS for 15 min and placed in six well-plates. The cell suspension was then added to the scaffolds, 50 µl on one side of each scaffold, and incubated for 15 min in a 5% CO<sub>2</sub>, 37°C incubator to allow initial attachment. The seeded scaffolds were subsequently turned over and the procedure repeated. After the second incubation period, 5 ml of supplemented Dulbecco's modified Eagle's medium growth medium was added to each well and precultured for 7 days (medium change on day 3).

## Effect of mean pore size on cell density and cellular proliferation

Cell number was quantified using a Hoechst (Sanfrancisco, CA, USA) dye 33342 assays [17]. Hoechst 33342 (2'-[4-ethoxyphenyl]-5-[4-methyl-1-piperazinyl]-2,5'-bi-1H-benzimidazole

trihydrochloride trihydrate) is a cell-permeable DNA stain that is excited by ultraviolet light and emits blue fluorescence at 460-490 nm. Hoechst 33342 binds preferentially to adenine-thymine (A-T) regions of DNA. This stain binds into the minor groove of DNA and exhibits distinct fluorescence emission spectra that are dependent on dye: base pair ratios. Hoechst 33342 can be used to quantitate DNA in solution. This stain is commonly used to identify replicating cells. Cell-seeded scaffolds and free cell were taken out of culture and washed in PBS before digesting in a solution containing 0.5 EDTA, cysteine-HCL, and 1 mg/ml papain enzyme (Sigma-Aldrich). The Hoechst staining solution was prepared by diluting the Hoechst stock solution 1: 2000 in PBS. The staining solution was added to cover the cells. Incubation was done for 5–10 min and protected from light. The staining solution was removed. The cells were washed three times in PBS. Measurements were taken using a fluorometric plate reader at an emission of 460 nm and excitation of 355 nm, 1.0 s. To

determine the initial cell attachment from the cell number, the percentage of cells present in the scaffolds after 24, 48, and 72h relative to the number of cells initially seeded onto the scaffolds at day 0 was calculated.

#### Effect of scaffold mean pore size on cell morphology

Using SEM, seeded scaffolds were imaged after 7 days of culture to investigate whether the morphology of cells was affected by scaffold's mean pore size. In detail, the cell morphology of 7-day-old cells was examined on the prepared scaffolds by washing three times with PBS buffer and once with distilled water. After that, the cells were fixed on the scaffold surface by using 4% glutaraldehyde and dehydrated in a graded ethanol solution (15, 25, 35, 45, 70, and 95% ethanol) each for 10-20 min. Samples with cells were attached to stubs and coated with an ultra-thin layer of gold in a coating apparatus, and then the morphology of cells was observed by SEM with EDS.

#### Effect of mean pore size on odontogenic gene expression

To determine gene expression on the cultured cells within the scaffolds, real-time reverse transcription PCR (RT-PCR) reactions were carried out. The total RNA was extracted from the cultured cells, and RT-PCR was performed to analyze the mRNA level of odontoblastic differentiation marker gene, dentin sialophosphoprotein (DSPP) (Lonza, USA) [18]. In brief, the total RNA was isolated using an RN easy kit (Qiagen, Crawley, UK) using established methods. Particularly, 40 200 ng of total RNA was reverse transcribed to cDNA using a QuantiTect reverse transcription kit (Qiagen) on an authorized thermal cycler (Mastercycler Personal; Eppendorf, Kontich, Belgium). RT-PCR were run on the 7500 RT-PCR System (Applied Biosystems, Joeil, Japan) using a QuantiTect SYBR Green PCR kit (Qiagen). The relative expression of mRNA was calculated by

 $\Delta\Delta C_{\rm t}$  method with a house-keeping gene, GAPDH. The target gene chosen was DSPP. This targeted gene was chosen as it is expressed in cells differentiating down the characteristic odontogenic lineage.

#### Statistical analysis

Statistical differences between different types of the scaffold were assessed by two-way analysis of variance and Tukey's post-hoc analysis. Statistical differences between the two treatments were assessed by Student's paired-wise sample and independent sample t-test. All results were reported as the mean±SD. A probability value of 95% ( $P \le 0.05$ ) was used to determine significance. Statistical analysis was performed with IBM SPSS version 20 for Windows, Munich, Germany [18].

#### Results

## Transmission electron microscope of 58S bioactive

The prepared bioactive glass 58S was examine under transmission electron microscope, in which the morphology of the nanoparticles of the product is composed of agglomerations of semi-spheres. Their diameter ranged between 23.90 and 98.18 nm. Moreover, it was extremely obvious that nanoparticles were showing smooth surfaces of the particles, confirming their amorphous structure (Fig. 1a).

#### Thermal behavior of the prepared bioactive glass (DSC and TGA)

The DSC/TGA graph was used to demonstrate the thermal properties of the powder samples examined in the stability of a molecule at high temperatures, that is, the molecule with greater stability has more resistance to degradation at high temperatures (Fig. 1b and c).

The prepared bioactive glass showed characteristics peaks, the first peak at 550°C as the temperature of vitreous transition (Tg), at 720°C as the



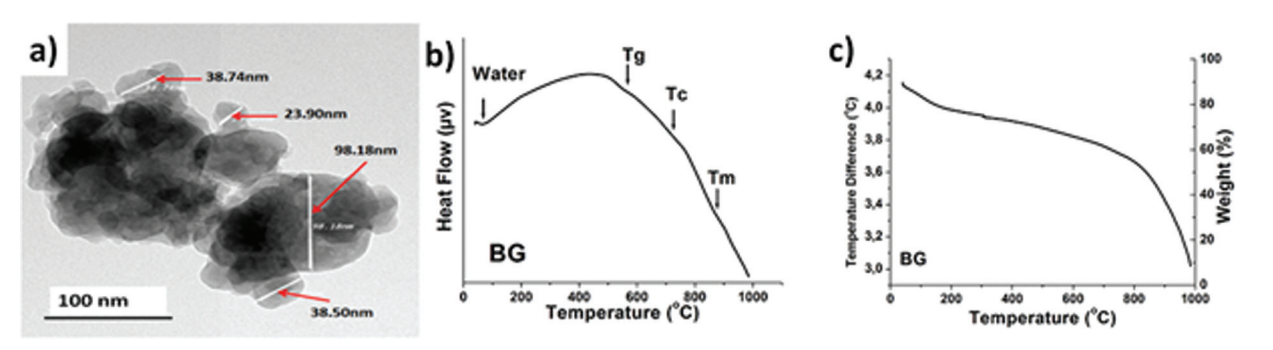


Illustration of (a) transmission electron microscopy image, (b) DSC, and (c) TGA of the prepared 58S bioactive glass by sol-gel method.

86

temperature of crystallization (Tc), and at 885°C as (Tf) temperature of fusion. The thermal stability [(Tc-Tg)=(720-550.6)] was  $170^\circ$ ; thus, it indicated lower thermal stability for the prepared bioactive glass when compared with the early reported thermal stability of bioactive glass. The obtained thermal stability would, in turn, disturb the chemical stability of the bioactive glass (more reactivity) which in turn would enhance its bioactivity. The TGA results were found to be correlated with the DSC results, particularly, 40-60% of the bioactive glass was decomposed in a heating range of 550-750°C corresponding to both recorded temperatures Tg and Tc. In addition to that approximately 30% decomposition of the bioactive glass was detected at heating range of 750-900°C, which was assigned to the melting interaction.

#### X-ray diffraction

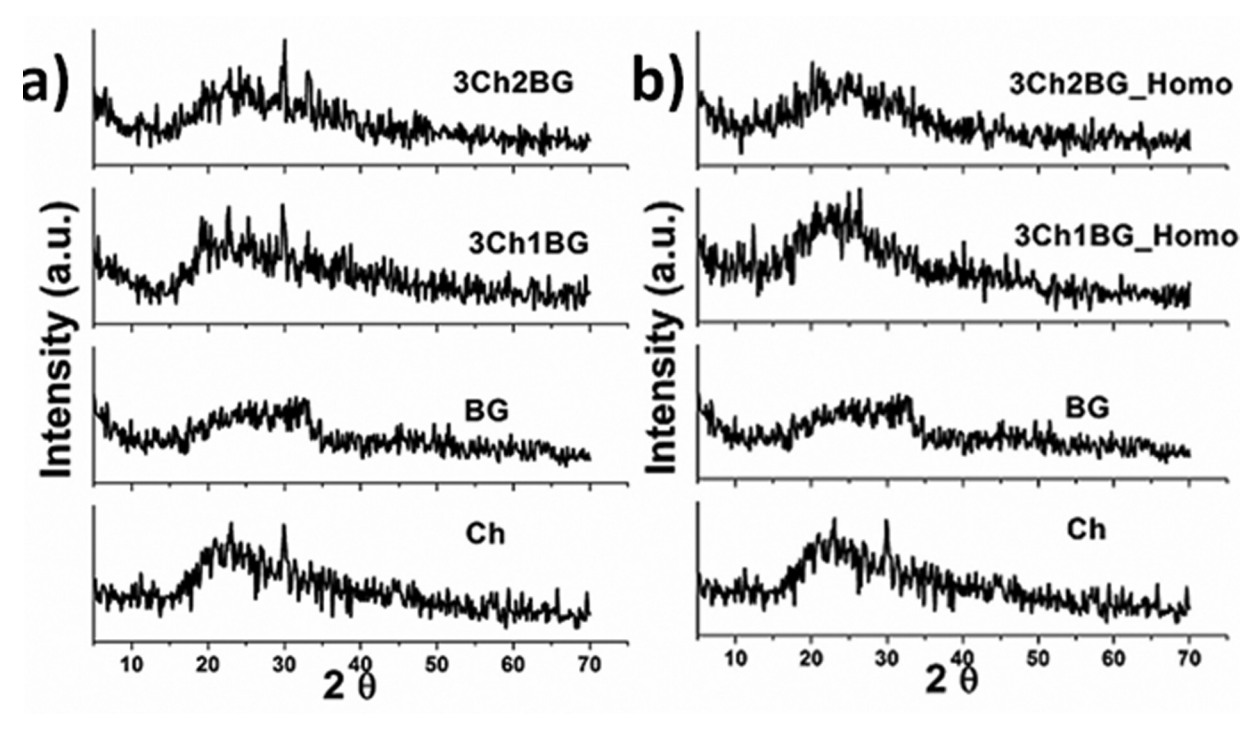
The prepared nanocomposite scaffolds with reference to their native component were investigated using XRD analysis to determine the effect of preparation method as well as the presence of bioactive glass on their phases. Figure 2a represents the XRD patterns of chitosan, prepared nano-bioactive glass 58S, and two types of heterogeneous three-dimensional (3D) porous scaffolds nanocomposite. It was worthy highlighted that the XRD pattern of pure chitosan (Ch) exhibited a semi-crystalline curve that was considered as the characteristic profile of the chitosan structure. The XRD pattern of the prepared nano-bioactive glass

58S represented in Fig. 2a and b demonstrated an amorphous broad peak in the range of 18°–35°. In addition, there are no detectable crystalline peaks in the pattern. The XRD patterns of prepared nanocomposites (3Ch1BG and 3Ch2BG) demonstrated that there were very board humps diffraction peaks for all samples after the loading of bioactive glass, which specified the noncrystalline structure of the 58S glass and the prepared scaffolds as observed from the absence of sharp peaks with delectable diffraction peaks of chitosan.

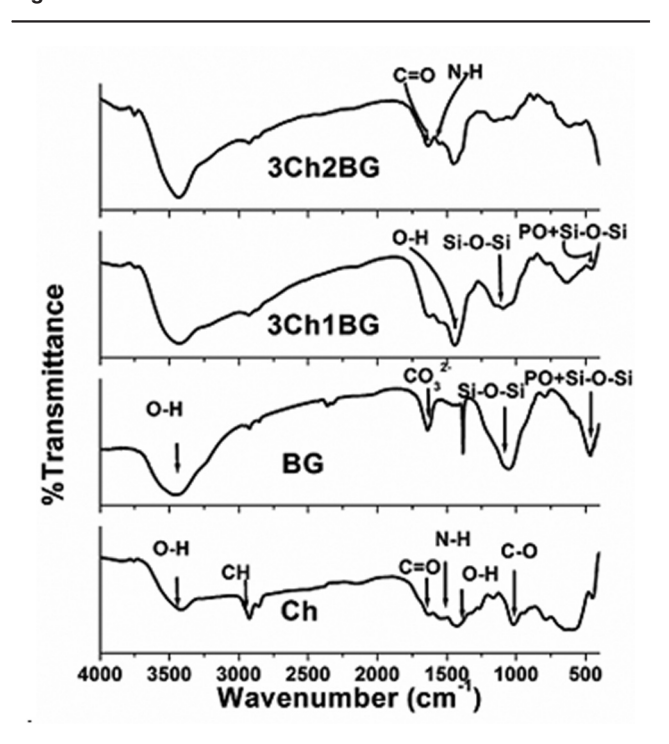
#### Fourier transform infrared spectroscopy analysis

The characteristic peaks of pure chitosan, bioactive glass 58S, and nanocomposite scaffolds were measured by FTIR analysis, and their spectra are represented in Fig. 3. In the FTIR spectrum of pure chitosan methylene (CH<sub>2</sub>), amide I (C=O), amino (NH<sub>2</sub>), and amide II (-NH) functional groups were detected at 2917, 1642, 1456, and 1552 cm<sup>-1</sup>, respectively. These bands were clearly noted in all nanocomposites. Moreover, phosphate groups of the bioactive glass were confirmed by the presence of absorption bands recorded at 1099, 952, 839, and 563 cm<sup>-1</sup>, whereas presence of OH group was affirmed by the stretching band detected in the range of 2900-3700 cm<sup>-1</sup>. Bands detected at 1457 and 1433 cm<sup>-1</sup> confirmed the presence of carbonate groups. Figuring out the chemical structure of silicate glasses was conduct utilizing FTIR spectroscopy,

Figure 2



X-ray diffraction curves of (a) the heteroporous scaffolds and (b) the homoporous scaffolds.



The Fourier transform infrared spectroscopy spectra measured for chitosan, 58S nano-bioactive glass, and nanocomposite three-dimensional scaffolds.

which is considered as a substantial characterization tool for this purpose. Thus, the formation of Si-O-NBO groups that occurs upon the breakage of Si-O-Si bonds is an indication parameter in evaluating the alterations that takes place to Si-O-Si vibration modes. The biological response at the interface of the bioactive materials when exposed to body fluids is usually explained by these groups. The absorption bands of bioactive glass 58S (BG) were identified as follows. Moreover, the bands detected at 480 cm<sup>-1</sup> and around 731 cm<sup>-1</sup> indicate the presence of Si-O bending mode functional group. The P-O bending mode band was also observed at 602 cm<sup>-1</sup>.

Moreover, the band at 926 cm<sup>-1</sup> was associated with Si-O with one NBO. In addition, the band observed at 1037 cm<sup>-1</sup> that was attributed to Si-O asymmetric stretching mode was also detected. The band around 1637 cm<sup>-1</sup> that was related to molecular OH of water was observed. For nano-bioactive glass, silicate absorption bands assigned to peaks 1085, 800, and 464 cm<sup>-1</sup>, correspondingly, were detected. In addition to that, other peaks at 580 and 600 cm<sup>-1</sup> indicated a P-O bending vibration owing to the presence of phosphate group. Furthermore, 2Ch1BG 3Ch1BG nanocomposite scaffolds displayed the similar FTIR spectrum observed for pure chitosan scaffold (Ch) combined with the characteristic bands

for the bioactive glass as demonstrated in the aforementioned section. Thus, it confirmed the inclusion of the bioactive glass nanoparticles. However, it seems that the magnitude of these bands becomes weaker and broader with the development of all nanocomposites.

#### Scanning electron microscope before in-vitro study

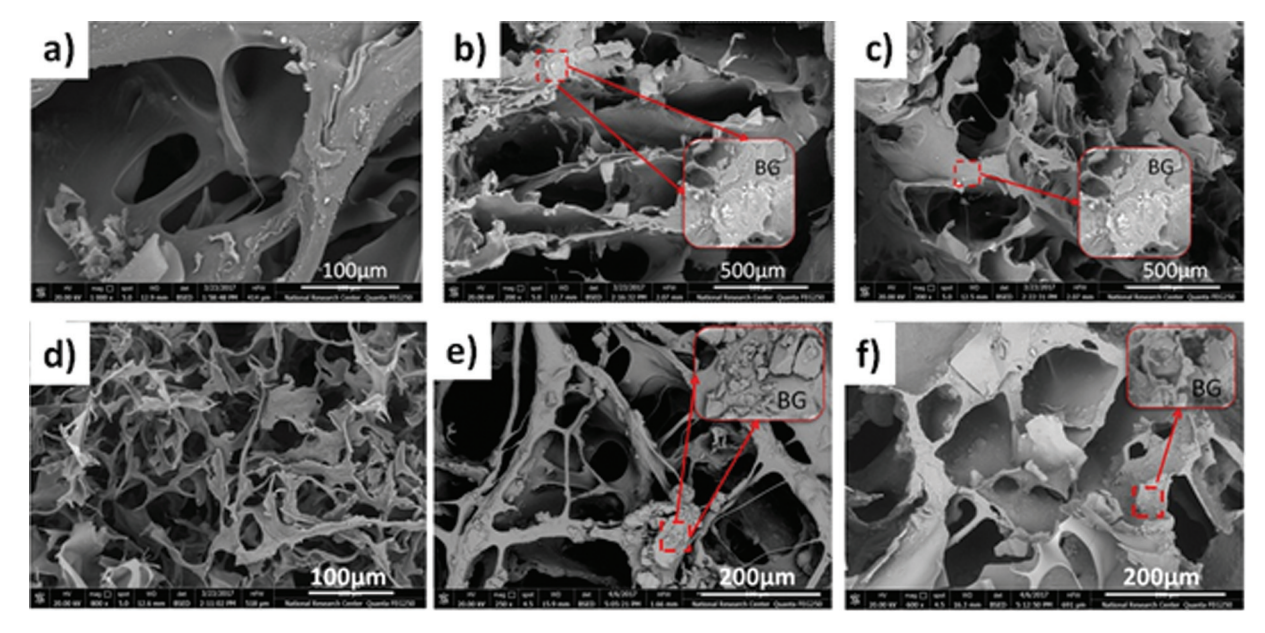
The SEM micrographs of the prepared scaffold composites (Ch, 2Ch1BG, and 3Ch1BG) are shown in Fig. 4a-c. Direct information about the designed porous structure of the nano-bioactive glass/chitosan scaffold nanocomposites could be assessed by the SEM images. Generally, in the SEM images, we can obviously note a large number of pores around the size of  $400-700 \, \mu m$ . These pores are connected to each other to form a coherent porous network, which directly affects the biological performance of the material.

The SEM micrographs of the prepared nano-bioactive glass/chitosan scaffold composites (homogenous) are shown in Fig. 4d-f. For pure chitosan scaffold prepared in the presence of H<sub>2</sub>O<sub>2</sub>, it is very obvious that the pores are distributed in semi-homogeneous distribution manure. The pores seemed to be interconnected, and this was also supported by the high porosity and high open pores content determined by pore size when compared with the nanocomposite scaffolds. Upon the inclusion of nano-bioactive glass, remarkable changes for the microstructure of the nanocomposite scaffold occurred. The pore sizes were around 300-700 µm for pure chitosan scaffold, but the pore size for the nanocomposite scaffold was smaller and the pore walls were thicker. The rough surface at all prepared composites began to be observed with incorporation of BG58S according to weight% of BG58S in composites. Moreover, it is clearly observed that the BG58S nanoparticles were embedded well in the chitosan matrix.

#### **Scaffold porosity**

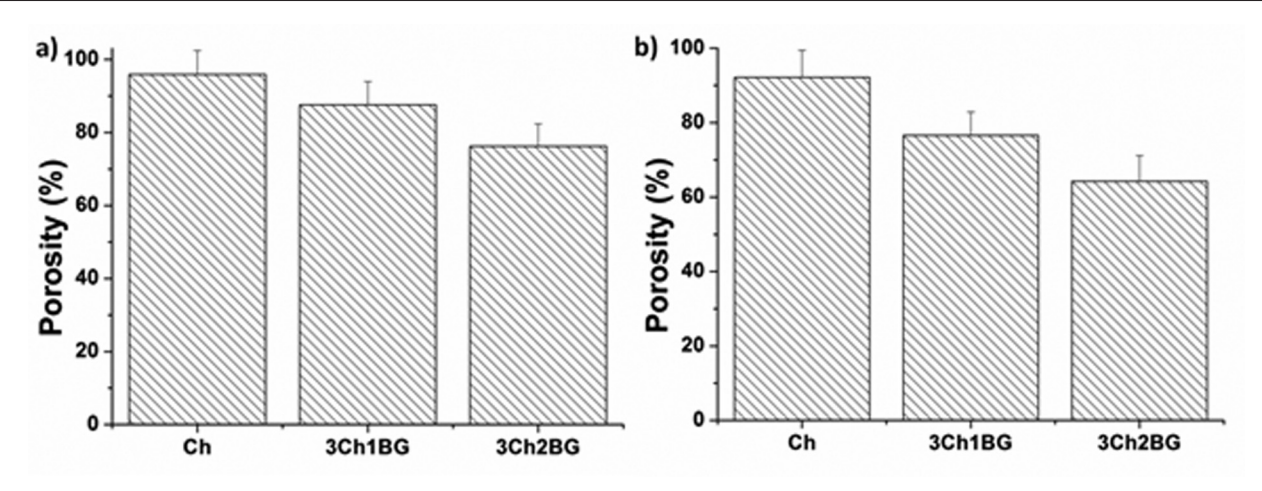
The scaffolds porosity (%) was determined by liquid displacement method, and the results are shown in Fig. 5. It is very clear that the higher porosity percentage was recorded for pure chitosan scaffold (E 90%) (Fig. 5a). The presence of the nanobioactive glass slightly decreased the porosity (%) for all the prepared nanocomposite scaffolds based on the glass concentration within the chitosan polymer matrix. It is worthy to note that the presence of H<sub>2</sub>O<sub>2</sub> has a slight effect on the decreasing of the porosity (%) for all the prepared nanocomposite scaffolds using H<sub>2</sub>O<sub>2</sub> (Fig. 5b).

Figure 4



Scanning electron microscope of (a) hetero chitosan, (b) hetero 3Ch1BG, (c) hetero 3Ch2BG, (d) homo chitosan, (e) homo 3Ch1BG, and (f) homo 3Ch2BG scaffolds.

Figure 5



Demonstration of the porosity (%) of the prepared scaffolds (a) heteroporous scaffolds and (b) homoporous scaffolds.

#### Mass loss (%) of the scaffolds

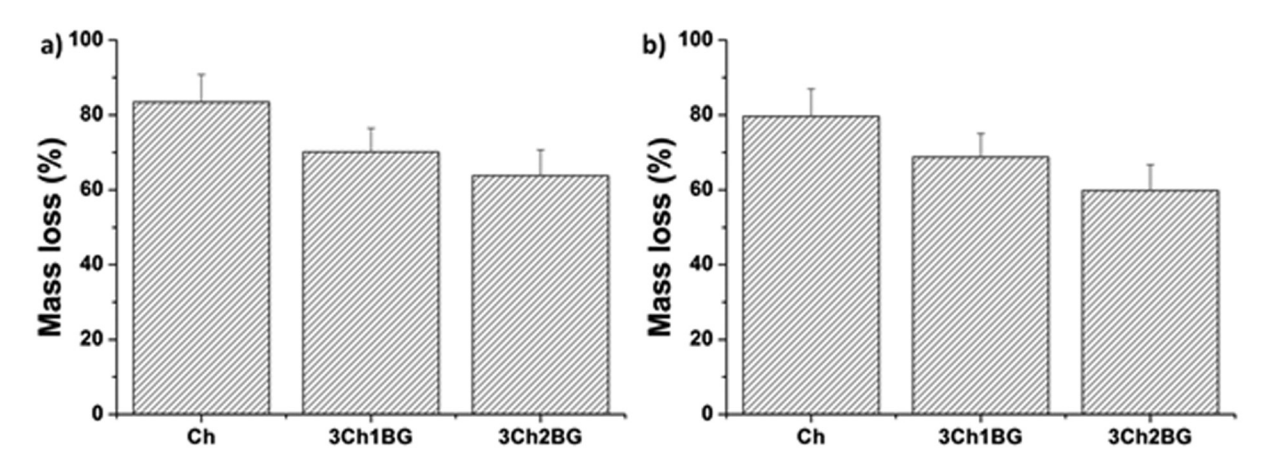
The mass loss (%) of all the degisned scaffolds was conducted in SBF, and the results were expressed in bargraphs represented in Fig. 6. The mass loss (%) of prepared scaffolds was found to be slightly affected by the presence of bioactive glass. In details, higher mass loss (%) was assigned to pure chitosan (? 80%) after 28 days of soaking in SBF (Fig. 6a). However, the relative decrease in mass loss (%) was measured for the nanocomposite scaffolds loaded with nanobioactive glass (? 80%) based on the glass concentration loaded in the chitosan polymer matrix. A very minor decrease in the mass loss (%) was recorded for the scaffolds prepared in the presence of  $H_2O_2$  (Fig. 6b).

#### **Cells** isolation

Stem cells were successfully isolated from DPSC, in which the tissues were treated enzymatically, and stem cells were successfully isolated by their ability to adhere to plastic plates. Following the isolation and culturing procedures, the stem cells from DPSC began to attach to the bottom of the culture dishes. The cultured cells were observed on a regular basis using an inverted light microscope. The cells appeared with various spindle-like morphologies, some (fibroblastic) appearance and others appeared stellate-shaped cells.

#### Subculturing (passaging)

Following confluence, the cells were passed successfully up to the third passage (P3). Subcultures tended to



Bargraphs showing the mass loss (%) of the prepared scaffolds (a) heteroporous scaffolds and (b) homoporous scaffolds.

exhibit accelerated growth, so the cultures reached confluence in a shorter time than primary cultures (in about 5-6 days). During expansion cultures, HHDPSCs in passage one (P1) showed an increase in the number of cells which maintained their spindle shape. In passages 2 (P2) and passage three (P3), the number of cells kept increasing (Fig. 7a and b). Cells in later passages showed an increase in the number of compressed cells that lost their spindle shapes (Fig. 7c and d).

#### Assessment of stemness after isolation by flow cytometry

Using flow cytometric analysis, the expressions of CD90, CD105, and CD45 were quantified. The flow cytometric analysis revealed that HHDPSCs were positive for CD90. On the contrary, all types of cultures were negative for the leukocyte precursor marker CD45.

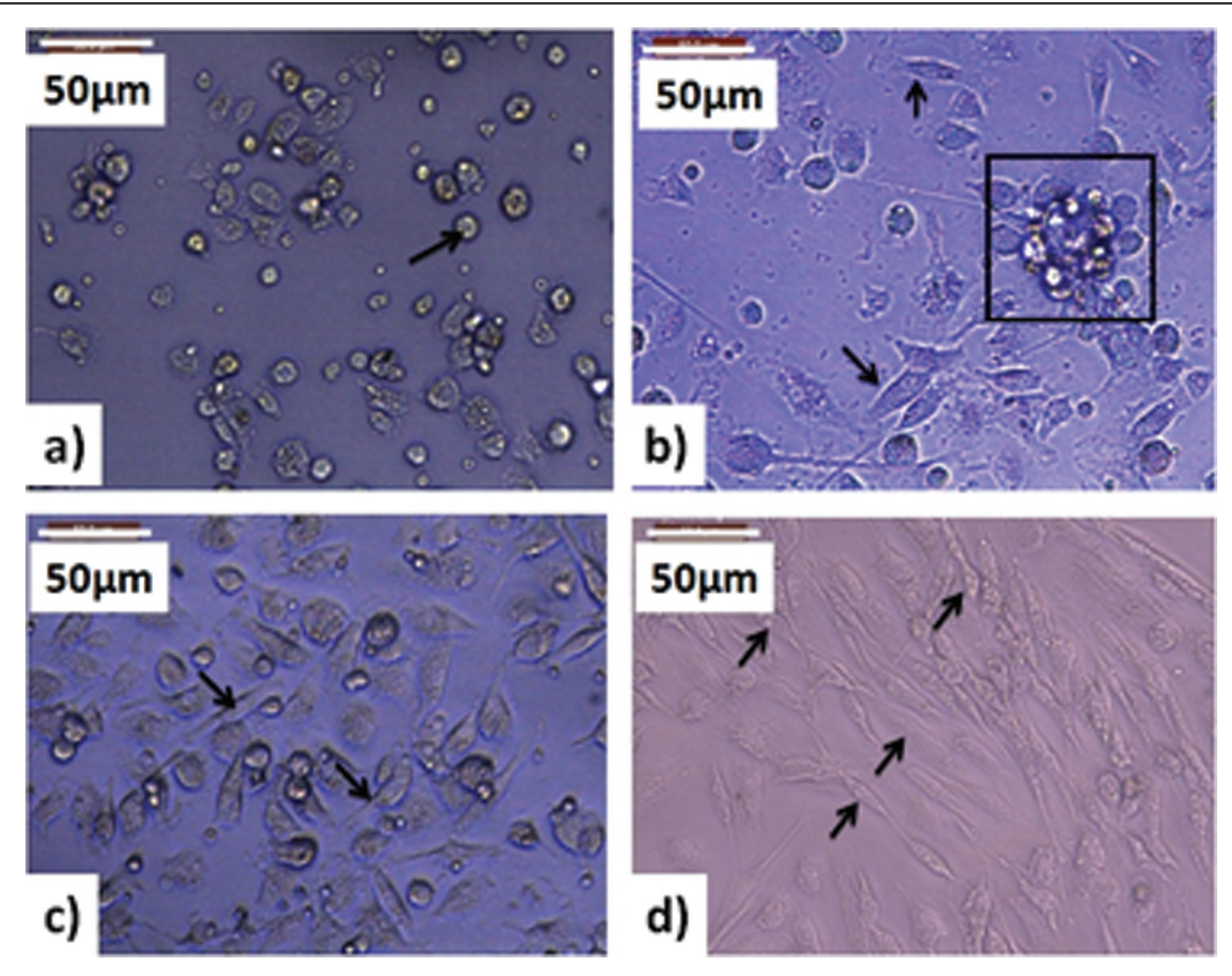
#### Scanning electron microscope-energy-dispersive X-ray spectrometry after in-vitro study

The SEM of all prepared scaffolds after embedding invitro with dental stem cells for 7 days are represented in Fig. 8. In Fig. 8a, a bone nodule was observed on Ch scaffold. indicating the emergence of a matrix outside the fibrous and matrix vesicles, whereas the SEM showed elucidating foci of mineralization in the form of calcified nodules (Fig. 8b).

SEM results in Fig. 8a showed obvious cell-matrix interactions of the dental stem cells with heterogeneous chitosan scaffold (Ch). The cell processes interacting with the scaffolds and forming many mineralized nodules on the surface are obtained in Fig. 8a. From the SEM of heterogeneous Ch scaffold, it can be noted that dental stem cells were attached, survived, multiplied, and interacted with their extracellular environment when cultured within the scaffolds. This indicated that the cells have grown well, secreted extracellular matrix (ECM), mineralized nodules on the wall of pores of the 3Ch1BG heterogeneous scaffold.

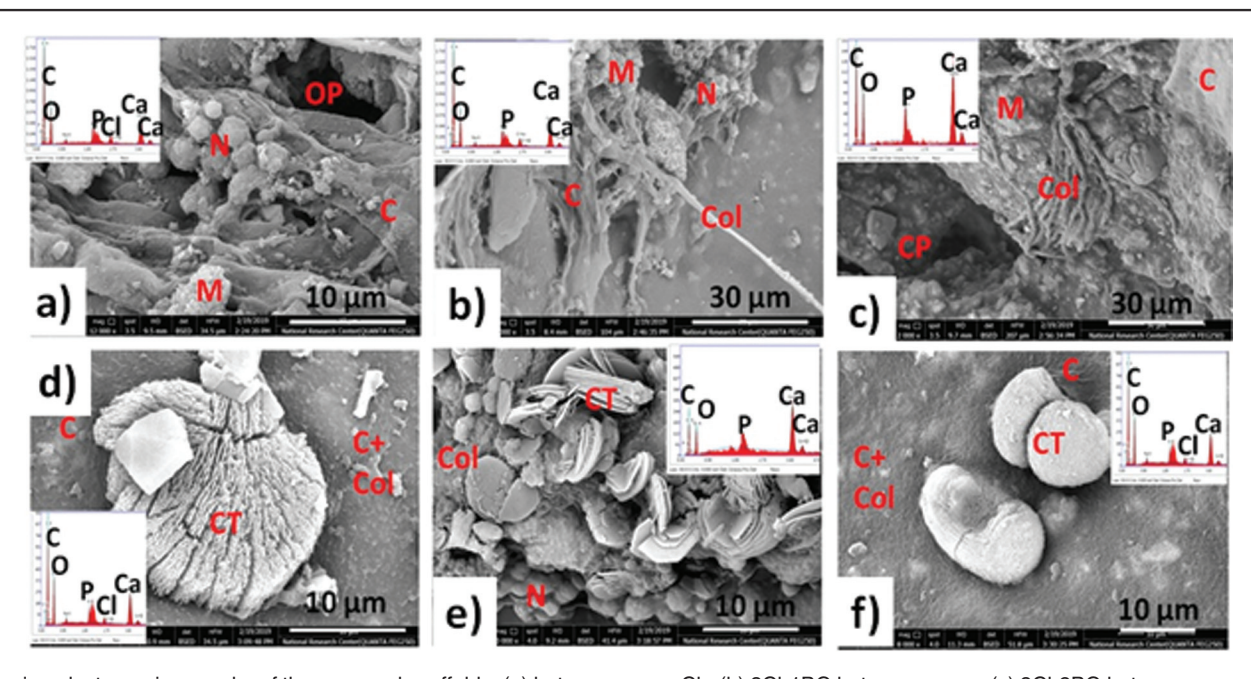
Accumulation of nodules was formed also over the 3Ch2BG heterogeneous scaffold, and there was a network of overlapping layers of cells overlapping boundaries and interrelated processes (Fig. 8c). Moreover, the cells seemed to be flattened and well propagated, covering the surface of the scaffold and migrating into the inner pores of the 3Ch2BG heterogeneous scaffold (Fig. 8c). The EDS analysis of the surface of the seeded dental stem cells on heterogeneous scaffolds with human pulp MSCs for 7 days (Fig. 8a-c) has detected the presence of Ca and P elements on the surface. Moreover, a dentin-like structure nodule was noted on the surface of homogeneous chitosan scaffold (Fig. 8d). Many clusters of organized crystalline round plates were distributed homogeneously over almost all of the surface of all homogeneous 3Ch1BG scaffolds (Fig. 8e); these clusters have closed all the pores of the homogeneous scaffolds. Furthermore, SEM of 3Ch2BG homogenous scaffold showed a clear indication of the formation of well-organized crystals based dentin-like matrix deposition on the surface of all homogeneous scaffolds, thus reflecting probably the early odontogenic differentiation stage of the dental pulp stem cells. The EDS analysis of the surface of the seeded dental stem cells on homogeneous scaffolds with human pulp MSCs for 7 days (Fig. 8d-f) has detected the presence of Ca and P elements on the surface of all homogeneous scaffolds. We noted that the heterogenous scaffolds were characterized by high

Figure 7



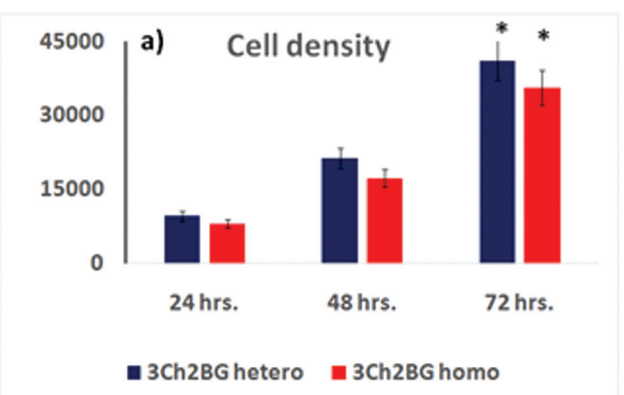
Mesenchymal stem cells-derived dental pulp after (a) 24 h culture, (b) 48 h culture, (c) 72 h culture, and (d) 72 h culture (passage 1); black arrow represented the spindle-shaped cells. Black square represented the colony-forming unit with spindle cells emerged beneath it (scale bar:  $50 \mu m$ ).

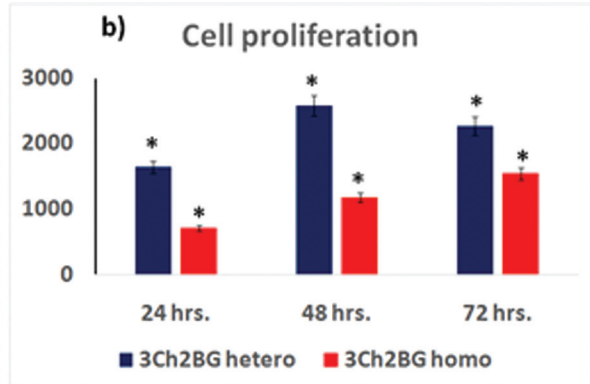
Figure 8



Scanning electron micrographs of the prepared scaffolds: (a) heterogeneous Ch, (b) 3Ch1BG heterogeneous, (c) 3Ch2BG heterogeneous, (d) homogeneous Ch, (e) 3Ch1BG homogeneous and (f) 3Ch2BG homogeneous scaffolds incubated with dental stem cells for 7 days; C, cells; Col, collagen; CP, closed pores; M, mineralized extracellular matrix; N, nodules; OP, open pores.

Figure 9





Demonstrate (a) cell density and (b) cell proliferation for homoporous and heteroporous 3Ch2BG scaffolds.

dentin-like matrix deposition more than the homogeneous scaffolds.

#### Effect of scaffold mean pore size on cell density

The cell density and proliferation were determined for heteroporous and homoporous 3Ch2BG scaffolds as they showed the best cell attachments and calcified tissues. Differences in pore structure resulted in a linear relationship between the average pore size of scaffolds and cell density of HDPSCs over 24, 48, and 72 h period as well as an increase in the total density in each time interval. The highest mean value was found in 72 h followed by 48 h, whereas the lowest mean value was found in 24 h (Fig. 9a).

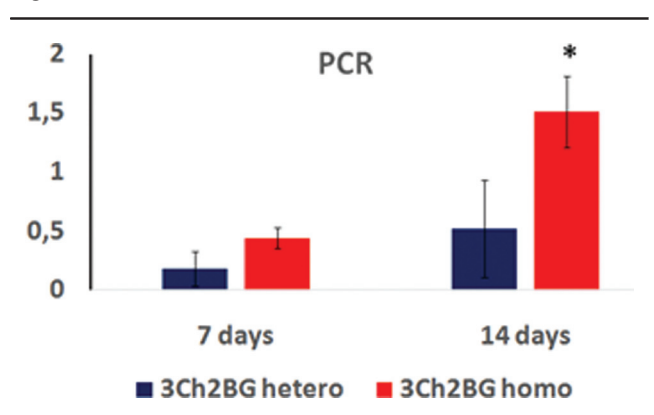
#### Effect of scaffold mean pore size on human dental pulp stem cells proliferation

The in-vitro response regarding proliferation of HDPSCs to the different mean pore size was estimated and detected a strong linear association of rising proliferation with larger mean pore size through 24, 48, and 72 h, where statistically, the highest mean value was found in 3Ch2BG hetero, whereas the lowest mean value was found in 3Ch2BG homo. A statistically significant difference was found between 3Ch2BG hetero and 3Ch2BG homo at 24 and 48 h (P<0.001), whereas no statistically significant difference was found between 3Ch2BG hetero and 3Ch2BG homo at 72 h (*P*=0.052), as shown in Fig. 9b.

#### Effect of scaffold mean pore size on human dental pulp stem cells differentiation

Gene expression analysis by PCR showed that scaffold mean pore size significantly affected odontogenic gene expression. Heterogenous scaffolds with the largest mean pore size stimulated approximately two-fold higher DSPP gene expression than the smallest pore size homogenous scaffold respectively after 7 days. A statistically significant

Figure 10



Gene expression of the selected scaffolds determined using PCR.

difference was found between 3Ch2BG hetero and 3Ch2BG homo, where P value less than 0.001. The highest mean value was found in 3Ch2BG hetero, whereas the lowest mean value was found in 3Ch2BG homo, as shown in Fig. 10.

#### Discussion

Tissue engineering is governed by three basic parameters; these parameters include inducting signals, responsive cells, and a matrix/scaffold [19]. Biomaterials perform an imperative job in coordinating tissue regeneration, and chemical properties of the scaffolds have been appeared to affect the conduct of undifferentiated cells, whereas the scaffold synthesis has a critical job in stem cell maturation toward a favored passage [8].

In addition, stem cell performance depends on the scaffold's locative properties, for example, pore size, percentage porosity, and void fraction. Scaffold's pore diameter has appeared to influence the biological aspects of stem cells. So, 3D architecture is a pivotal role in tissue engineering and regenerative medicine [20].

TEM of bioactive glass 58S revealed that it is in nanoscale. XRD of bioactive glass confirmed its amorphous nature [21]. The XRD of the prepared scaffolds revealed that incorporation of the bioactive glass did not alert the physical stability and amorphous nature of obtained scaffolds [22]. FTIR spectra of all prepared scaffolds mentioned bands were reported for chitosan and bioactive glass 58S. Functional groups of chitosan and bioactive glass 58S were studied using FTIR spectra which exhibited that the absorption bands broadened with adding of the bioactive glass [22]. Permeable structure empowers the growth of cells into pores, giving enough sustenance and blood supply through infiltration and dissemination. The reason for the permeable morphology is that in the solidified procedure, nanocomposites are expelled into the holes among the ice crystals [22,23]. The rough surface at all prepared composites began to be disturbed with the incorporation of BG58S according to the content percent of BG58S in composites. The nano-bioactive glass particles were embedded well in the chitosan matrix [22].

The evaluations of biological performance are also reported in the current research, in concern with cell proliferation, and differentiation seeded and cultured onto the newly **HDPSCs** developed chitosan/nano-bioactive 58S glass scaffolds prepared in presence and absence of H<sub>2</sub>O<sub>2</sub>. Different solubilizing media for preparation of the current scaffolds using freeze-dryer allowed us to obtain 3D porous structures. The porosity (%), pore size distribution, and mass loss (%) were found to be controlled with bioactive glass concentration as well as H<sub>2</sub>O<sub>2</sub>. Every single created scaffold was found to be noncytotoxic to HDPSCs, as the leachables discharged during the extraction time frame did not influence cell viability and did not cause changes in cell morphology. Cells had the capacity to colonize the 3D structures up to 21 days, and these outcomes were in a similar line with past announced investigations [24-30]. The cell multiplication was progressive and ceaselessly expanding till the end of culture time, confirming the newly developed chitosan/nano-bioactive glass 58S scaffolds [24]. The differences observed for the different types of the prepared scaffolds are likely attributed to the diverse chemistry of the surface and pores diameter of the 3D structures, with the best outcomes being seen for the scaffolds created from developed homogeneous chitosan/nanobioactive glass 58S scaffolds [24].

Alkaline phosphatase is considered to be one of the early markers for cell differentiation for cells that are

undergoing osteodentic differentiation [31,32], not being specific for the dental pulp stem cells. Alkaline phosphatase is utilized normally to show the early differentiation into a dentin-related phenotype, which is seen by the expansion of the enzyme action until the second week. The Ca and P precipitates on the scaffold surface seeded with stem cells indicated the development of mineralized ECM. This reality is in concurrence with the information acquired for basic phosphatase tests, demonstrating had experienced an differentiation in earlier culturing time and were forming mineralized ECM [15,33].

Cell adhesion is a multistage process that includes physicochemical reactions, mediated by different factors, such as the behavior of the cells and the characteristics of the scaffold surface (roughness, softness, chemical composition, hydrophobicity, and charge). The adhesion of the cells to a scaffold surface regularly controls the cell behavior especially their proliferation, spread, morphology, signaling, migration, and ECM deposition [33]. To explore the biocompatibility of the scaffold, we assayed the cell attachment (migration, adhesion, proliferation, spread, multilayer development, and invasion). These cell/scaffold interactions were analyzed by SEM after the scaffold/and cells were co-cultured for 7 days. The findings illustrated that heterogeneous scaffolds induced the attachment of remaining viable cells to its surface, whereas the homogeneous scaffolds showed high mineralization to their surfaces.

The prepared heterogeneous scaffolds exhibited the highest cell adhesion with effective cell adhesion, growth of multilayer cells, and invasion. The attached cell layer to the surface of the scaffold represents the evidence of its adhesion and biocompatibility [33]. For cell infiltration to occur, the pore size of a scaffold should be greater than the size of a cell. It was reported that the minimum pore size necessary for cellular infiltration to occur is  $10 \, \mu m$ [34]. Accordingly, our results for the prepared heterogeneous scaffolds can be explained by the largest pore size and the highest porosity as compared with the prepared homogeneous scaffolds. All prepared scaffolds in our study have a pore size close to the minimum pore size suggested by Zhang et al. [34] that is required for cell infiltration or migration. Moreover, increasing the scaffold surface porosity seems to have a significant role in the spreading and in the invasion of the cells, and also in improving the biocompatibility [33,34]. Despite no favored material for scaffold exists in regenerative endodontics, a

chitosan-based platform may turn out to be best owing to the fact that chitosan displays numerous properties good to new pulp and dentin structuring. In addition, it possesses modifiable porosity to allow transport of supplements, biomolecules, and poisonous cell waste. Its compression strength and biodegradability could be modified, and it is nontoxic, antibacterial, angiogenic, and impervious to endotoxin and bacterial corruption [35,36].

It is worth to highlight that the choice of scaffold depends on the specific tissue to be engineered. It is generally recognized that chemical properties of materials can influence the cellular behavior of SEM images odontoblasts. for the investigated scaffold suggested that the homoporous scaffold had higher support for odontogenic activity, and these results were in the same line with early reported studies [15,33]. The finer the pore diameter for 3D structures, the higher noteworthy the surface area for cell adhesion on its surface; nevertheless, the cell infiltration can be decreased. Moreover, it has a direct effect on the dispersion of supplements and evacuation of waste within the scaffold, leading to the formation of necrotic areas inside the 3D structure. From other respect, the bigger the pore diameter for 3D structures, the simpler the traffic of supplements, gas dispersion. and removal of metabolic waste; in any case, it diminishes the relative surface for cell adhesion [37]. It is interesting to point out that scaffold pore size affects other HDPSCs behavior plus cellular density and attachment. In this context, profound analysis conceded to determine proliferation as well as cellular differentiation. In particular, heterogenous scaffolds with large pore size stimulated the highest value of cellular proliferation in comparison with homogenous scaffolds with small pore size at each time point of the study. This was consistent with other observation detected in Wang et al. [38] which recommended that bigger mean pore diameter provide more cell adhesion and in this manner more prominent proliferation which may have an impressive implication for differentiation.

When the cell morphology was assessed in the 3D chitosan scaffold at different time point (24, 48, and 72 h) upon the cell seeding, it was obvious that morphology of the seeded cells varied with modified scaffold mean pore diameter, whereas the initial attachment mechanism may influence the state of the cells inside the 3D structure, as big heterogenous mean pore diameter possibly representing fewer ligands for cell attachment, along these lines allowing adjusted morphologies which are attributes of an odontogenic phenotype. On the contrary, scaffolds with small homogenous mean pore size may allow flat cell attachment. This finding is in accordance with Matsiko et al [16].

The most notable result from this study is that change in the mean pore size of the scaffold affected the expression of gene-specific for odontogenic differentiation, whereas heterogenous scaffold with large mean pore size stimulated higher DSPP gene expression compared with homogenous scaffold with small mean pore size. This finding was in agreement with the result of Matsiko et al. [16] and Oh et al. [39] who confirmed that a scaffold with large mean pore size enhanced microenvironment provides odontogenic differentiation of HDPSCs with a significantly higher level of DSPP than scaffold with small mean pore size. In this research work, it is concluded that the microstructure of 3D chitosan with nano-bioactive glass scaffold serves to support and regulate cellular behavior of HDPSCs such as cell seeding, migration, attachment, and proliferation. Moreover, this 3D scaffold with high porosity was shown to be capable of directing HDPSCs differentiation toward odontogenic lineages. Thus, comprehension examination and components by which scaffold engineering influences the interaction between scaffold and cells and consequent dentine tissue arrangement is still very significance.

#### Conclusion

In this study, we conclude that the scaffolds with the biggest mean pore diameter invigorated higher cell expansion, soluble phosphatase, and mineralized dentine-like ECM generation in respect to the scaffolds with the finer mean pore diameter. This heterogeneous the and homogeneous microarchitecture of scaffolds plays a significant role in dental pulp stem cells differentiation and calcified tissue development. Along these lines, these results showed the significance of pore diameter and physical properties of biomaterials in affecting stem cellmediated odontoblast cells and may have suggestions in the improvement of cutting edge tissue regeneration techniques for the treatment of dentin deformity.

#### Acknowledgements

This study was supported by National Research Center, Dokki, Cairo, Egypt.

## Financial support and sponsorship

### Conflicts of interest

There are no conflicts of interest.

#### References

- 1 Petersen PE, Bourgeois D, Ogawa H, Estupinan-Day S, Ndiaye C. The global burden of oral diseases and risks to oral health. Bull World Health Organ 2005: 83:661–669.
- 2 Schmalz G, Galler KM. Tissue injury and pulp regeneration. J Dent Res 2011: 90:828–829.
- 3 Cordeiro MM, Dong Z, Kaneko T, Dong Z, Zhang Z, Miyazawa M, et al. Dental pulp tissue engineering with stem cells from exfoliated deciduous teeth. J Endod 2008; 34:962–969.
- 4 Lentzari A, Kozirakis C. Problems in the root canal treatment of premature teeth with open apex. Stomatologia (Athenai) 1989; 46:309–315.
- 5 McTigue DJ, Subramanian K, Kumar A. Case series: management of immature permanent teeth with pulp al necrosis: a case series. Pediatr Dent 2013; 35:55–60.
- 6 Bružauskaitė I, Bironaitė D, Bagdonas E, Bernotiene E. Scaffolds and cells for tissue regeneration: different scaffold pore sizes – different cell effects. Cytotechnology 2016; 68:355–369.
- 7 Gomez S, Vlad MD, Lopez J. Design and properties of 3D scaffolds for bone tissue engineering. Acta Biomater 2016; 42:341–350.
- 8 Rad RM, Atila D, Akgün EE, Evis Z, Keskin D, Tazkaner A. Evaluation of human dental pulp stem cells behavior on a novel nanobiocomposite scaffold prepared for regenerative endodontics. Mater Sci Eng C Mater Biol Appl 2019; 100:928–948.
- 9 Khoroushi M, Foroughi MR, Karbasi S, Hashimibeni B, Khadimi AA. Effect of polyhydroxybutyrate/chitosan/bioglass nanofiber scaffold on proliferation and differentiation of stem cells from human exfoliated deciduous teeth into odontoblast-like cells. Mater Sci Eng C Mater Biol Appl 2018; 89:128–139.
- 10 Demarco FF, Casagrande L, Zhang Z, Dong Z, Tarquinio SB, Zeitlin BD, Shi S. Effects of morphogen and scaffold porogen on the differentiation of dental pulp stem cells. J Endod 2010; 36:1805–1811.
- 11 Hashemi-Beni B, Khoroushi M, Foroughi M, Karbasi S, Khadimi AA. Tissue engineering: dentin – pulp complex regeneration approaches (a review). Tissue Cell 2017; 49:552–564.
- 12 Karageorgiou VD, Kaplan D. Porosity of 3D biomaterial scaffolds and osteogenesis. Biomaterials 2005; 26:5474–5491.
- 13 Nagahama H, Maeda H, Kashiki T, Jayakumar RT, Tamura FH. Preparation and characterization of novel chitosan/gelatin membranes using chitosan hydrogel. Carbohyd Polym 2009; 76:255–260.
- 14 Mabrouk M, Mostafa AA, Oudadesse H, Mahmoud AA, ElGohary MI. Effect of ciprofloxacin incorporation in PVA and PVA bioactive glass composites scaffolds. Ceram Int 2014; 40:4833–4845.
- 15 Tohamy KM, Mabrouk M, Soliman IE, Hanan H, Aboelnasr MA. Novel alginate/hydroxyethyl cellulose/hydroxyapatite composite scaffold for bone regeneration: in vitro cell viability and proliferation of human mesenchymal stem cells. Int J Biol Macromol 2018; 112:448–460.
- 16 Matsiko A, Gleeson J, O'Brien FJ. Scaffold mean pore size influences mesenchymal stem cell chondrogenic differentiation and matrix deposition. Tissue Eng Part A 2015; 21:486–497.
- 17 Murphy CM, Haugh MG, O'Brien FJ. The effect of mean pore size on cell attachment, proliferation and migration in collagen-glycosaminoglycan scaffolds for bone tissue engineering. Biomaterials 2011; 31:461–466.
- 18 Duffy GP, McFadden TM, Byrne EM, Sarah-Louise Gill SL, Eric Farrell E, O'Brien FJ. Towards in vitro vascularisation of collagen-GAG scaffolds. Eur Cell Mater 2011; 21:15–30.
- 19 Yusof MFH, Zahari W, Hashim SNM, Osman ZF, Chandra H, Kannan TP, et al. Angiogenic and osteogenic potentials of dental stem cells in bone tissue engineering. J Oral Biol Craniofac Res 2018; 8:48–53.

- 20 Lu HT, Lu TW, Chen CH, Mi FL. Development of genipin-crosslinked and fucoidan-adsorbed nano-hydroxyapatite/hydroxypropyl chitosan composite scaffolds for bone tissue engineering. Int J Biol Macromol 2019; 128:973–984.
- 21 O'Donnell MD. Predicting bioactive glass properties from the molecular chemical composition: glass transition temperature. Acta Biomater 2011; 7:2264–2269.
- 22 Mabrouk M, Mostafa AA, Oudadesse H. Bioactivity and drug delivering ability of a chitosan/46S6 melted bioactive glass biocomposite scaffold. InterCeram 2013; 62:444–450.
- 23 Lefebvre L, Chevalier J, Gremillard L, Zenati R, Thollit G, Assolant DB, Govin A. Structural transformations of bioactive glass 45S5 with thermal treatments. Acta Mater 2007; 55:3305–3313.
- 24 Martins T, Oliveira AAR, Oliveira AC, Boaventura TP, Barrioni BR, Costa-Júnior ES, Pereira MM. Novel 3D composites with highly flexible behavior based on chitosan and bioactive glass for biomedical applications. Mater Chem Phys 2017; 189:1–11.
- 25 Maji K, Dasgupta S, Pramanik K, Bissoyi A. Preparation and evaluation of gelatin-chitosan-nanobioglass 3D porous scaffold for bone tissue engineering, Int J Biomater 2016; 2016:1–14.
- 26 Prabhu M, Priscilla SR, Kavitha K, Manivasakan P, Rajendran V, Kulandaivelu P. In vitro bioactivity and antimicrobial tuning of bioactive glass nanoparticles added with neem (Azadirachta indica) leaf powder. Biomed Res Int 2014; 2014:1–11.
- 27 Nazemi K, Azadpour P, Moztarzadeh F, Urbanska AM, Mozafari M. Tissue-engineered chitosan/bioactive glass bone scaffolds integrated with PLGA nanoparticles: a therapeutic design for on-demand drug delivery. Mater Lett 2015; 138:16–20.
- 28 María VR, Eduardo RH. Advanced material. Bioceramics: from bone regeneration to cancer. Nanomedicine 2011; 23:5177–5218.
- 29 Zhang Y, Ouyang H, Lim CT, Ramakrishna S, Huang ZM. Electrospinning of gelatin fibers and gelatin/PCL composite fibrous scaffolds. J Biomed Mater Res 2005; B 72:156–165.
- **30** Burdick JA, Mauck RL. Biomaterials for tissue engineering applications: a review of the pas t and future trends. New York, NY: Springer 2010.
- 31 Chang HI, Wang Y. Cell responses to surface and architecture of tissue engineering scaffolds. Rijeka: Intech. 2011.
- 32 Lee SJ, San CJ, Park KS, Khang G, Lee YM, Lee HB. Response of MG63 osteoblast-like cells onto polycarbonate membrane surfaces with different micropore sizes. Biomaterials 2004; 25:4699–4707.
- 33 Filipowska J, Lewandowska-Łańcucka J, Gilarska A, Niedźwiedzki L, Nowakowska M. In vitro osteogenic potential of collagen/chitosan-based hydrogels-silica particles hybrids in human bone marrow-derived mesenchymal stromal cell cultures. Int J Biol Macromol 2018; 113:692–700.
- 34 Zheng X, Wang W, Liu S, Jinglei Wu J, Li F, Cao L, et al. Enhancement of chondrogenic differentiation of rabbit mesenchymal stem cells by oriented nanofiber yarn-collagen type I/hyaluronate hybrid. Mater Sci Eng C Mater Biol Appl 2016; 58:1071–1076.
- 35 Bellamy C, Shrestha S, Torneck C, Kishen A. Effects of a bioactive scaffold containing a sustained transforming growth factor-β1-releasing nanoparticle system on the migration and differentiation of stem cells from the apical papilla. Mater Sci Eng C Mater Biol Appl 2016; 42:1385–1392.
- 36 Kishen A, Shi Z, Shrestha A, Neoh KG. An investigation on the antibacterial and antibiofilm efficacy of cationic nanoparticulates for root canal disinfection. J Endod 2008; 34:1515–1520.
- 37 Conde CM, Demarco FF, Casagrande L, Nör JE, Tarquinio SB. Influence of poly-I-lactic acid Scaffold's pore size on the proliferation and differentiation of dental pulp stem cells. Braz Dent J 2015; 26:2.
- **38** Wang J, Mab H, Jin X, Hu J, Liu X, Ni L, Ma PX. The effect of scaffold architecture on odontogenic differentiation of human dentalpulp stem cells. Biomaterials 2011; 32:7822–7830.
- 39 Oh SH, Kim TH, Im GI, Lee JH. Investigation of pore size effect on chondrogenic differentiation of adipose stem cells using a pore size gradient scaffold. Biomacromolecules 2010; 11:1948–1955.